Electrocatalysis

International Edition: DOI: 10.1002/anie.201504815
German Edition: DOI: 10.1002/ange.201504815

Blending Cr_2O_3 into a NiO–Ni Electrocatalyst for Sustained Water Splitting

*Ming Gong, Wu Zhou, Michael James Kenney, Rich Kapusta, Sam Cowley, Yingpeng Wu, Bingan Lu, Meng-Chang Lin, Di-Yan Wang, Jiang Yang, Bing-Joe Hwang, and Hongjie Dai**

Abstract: *The rising H_2 economy demands active and durable electrocatalysts based on low-cost, earth-abundant materials for water electrolysis/photolysis. Here we report nanoscale Ni metal cores over-coated by a Cr_2O_3-blended NiO layer synthesized on metallic foam substrates. The Ni@NiO/Cr_2O_3 triphase material exhibits superior activity and stability similar to Pt for the hydrogen-evolution reaction in basic solutions. The chemically stable Cr_2O_3 is crucial for preventing oxidation of the Ni core, maintaining abundant NiO/Ni interfaces as catalytically active sites in the heterostructure and thus imparting high stability to the hydrogen-evolution catalyst. The highly active and stable electrocatalyst enables an alkaline electrolyzer operating at 20 mA cm^{-2} at a voltage lower than 1.5 V, lasting longer than 3 weeks without decay. The non-precious metal catalysts afford a high efficiency of about 15 % for light-driven water splitting using GaAs solar cells.*

Hydrogen (H_2) is considered a promising energy resource because of its high gravimetric energy density and zero emission of greenhouse gas.[1] However, H_2 production has largely relied on steam reforming, suffering from dependence on natural gas, high cost, and low purity.[1b,2] Alternatively, H_2 can be produced by water splitting, which can potentially benefit from abundant water resources and high H_2 purity.[3] An ideal picture depicts a closed cycle of H_2 production by water electrolysis/photolysis and H_2 consumption into water by H_2 fuel cells. The current limitation lies in the low efficiency of energy conversion because of the sluggish nature of the electrochemical reactions.[1a,c,d,3a,f,4] Electrocatalysts are required to expedite the reactions and increase efficiency,[3b,d,5] but the state-of-the-art catalysts (mostly based on platinum and iridium) suffer from scarcity and high costs. Existing earth-abundant catalysts used in industry require a much higher voltage to obtain a similar H_2 production rate.[3a,f,6] In acids, electrolysis currents of 0.6–2.0 A cm^{-2} require 1.75–2.20 V using Pt and Ir.[3a] In alkaline solutions, electrolysis currents of 0.2–0.4 A cm^{-2} require 1.8–2.4 V.[3a] Stability is another important criterion for evaluating electrocatalysts. Although non-precious metal-based catalysts with high activity have been developed, long-term stability has not been achieved to meet the standard of commercial electrolyzers.[3a,f] To date, active and stable earth-abundant electrocatalysts fabricated by a facile synthesis are still highly desired.

We recently showed that a Ni/NiO core–shell heterostructure affording similar activity as Pt for hydrogen-evolution reaction (HER) electrocatalysis.[3d] It was suggested that the NiO/Ni nanointerfaces are unique in expediting HER by stabilizing H atoms on metallic Ni and releasing the generated OH^- on NiO. However, the electrolyzer using NiO/Ni heterostructures exhibited a 20 mV decay per day. Here, inspired by stainless steel that resists rusting from chemical corrosion by blocking oxygen diffusion with a surface passive film of chromium oxide (Cr_2O_3),[7] we introduced Cr to form mixed Cr_2O_3 and NiO overcoats on Ni cores (Ni@Cr_2O_3-NiO). The resulting electrocatalyst (named "CrNN") showed unprecedented high activity and stability towards HER catalysis for water splitting with or without light assistance.

The catalyst was synthesized by hydrolysis of precursors at 90 °C, drop-drying the product to coat a Ni foam followed by annealing at 300 °C (see the Supporting Information). Scanning electron microscopy (SEM) images showed well-coated Ni wires in the Ni foam by a film of highly dispersed nanoparticles (Figure 1 a), in which Auger electron spectroscopy (AES) mapping suggested a uniform distribution of Ni, O, and Cr elements (Figure 1 a).

With the catalyst nanoparticles sonicated off from the Ni foam, scanning transmission electron microscopy (STEM) imaging showed 5–20 nm nanoparticles (Figure 1 b and Figure S1 in the Supporting Information). Atomic scale electron energy-loss spectroscopy (EELS) mapping (see the Support-

[*] M. Gong,[+] M. J. Kenney,[+] Dr. Y. Wu, Dr. B. Lu, Dr. M. Lin, Dr. D. Wang, Dr. J. Yang, Prof. H. Dai
Department of Chemistry, Stanford University
Stanford, CA 94305 (USA)
E-mail: hdai@stanford.edu
Dr. W. Zhou[+]
Materials Science & Technology Division
Oak Ridge National Laboratory, Oak Ridge, TN 37831 (USA)
R. Kapusta, S. Cowley
Alta Devices, Sunnyvale, CA 94805 (USA)
Dr. B. Lu
School of Physics and Electronics, Hunan University
Changsha, 410082 (China)
Dr. M. Lin
Green Energy and Environment Research Laboratories
Industrial Technology Research Insititute
Hsinchu, 31040 (Taiwan, ROC)
Dr. D. Wang
Department of Chemistry, National Taiwan Normal University
Taipei, 11677 (Taiwan, ROC)
Prof. B. Hwang
Department of Chemical Engineering
National Taiwan University of Science and Technology
Taipei, 106 (Taiwan, ROC)
[+] These authors contributed equally to this work.

Supporting information for this article is available on the WWW under http://dx.doi.org/10.1002/anie.201504815.

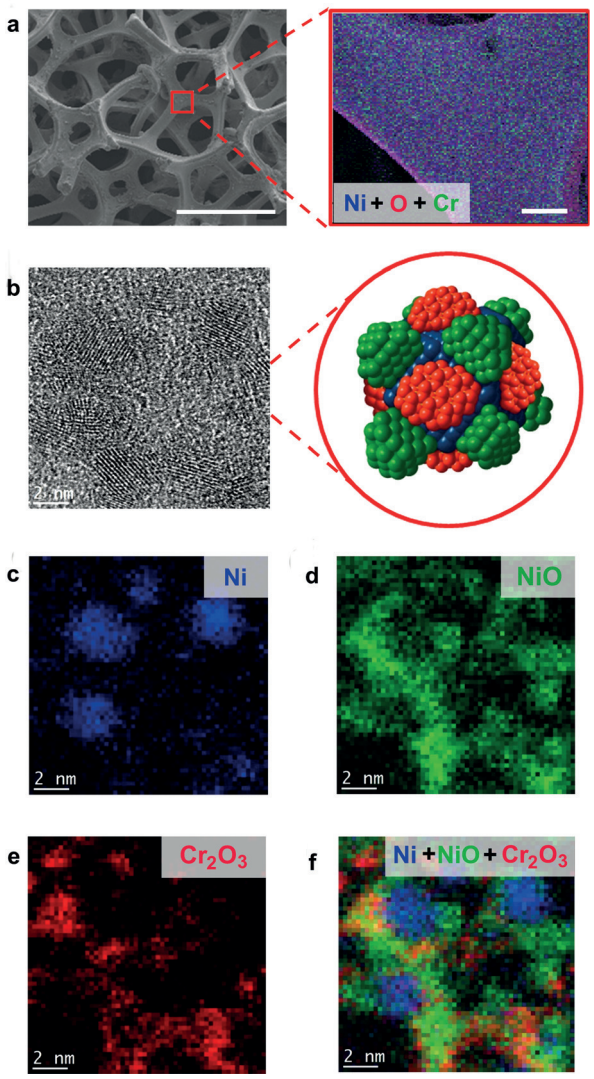

Figure 1. a) Low-magnification SEM image of the CrNN catalyst electrode with selected area AES elemental mapping showing uniform distribution of Ni, O, and Cr. b) High-resolution STEM bright-field image of the CrNN catalyst with its schematic illustration. c–f) High-magnification chemical maps by STEM-EELS spectrum imaging for the spatial distribution of Ni, NiO, Cr_2O_3 and their overlays showing Cr_2O_3-blended NiO/Ni heterostructures.

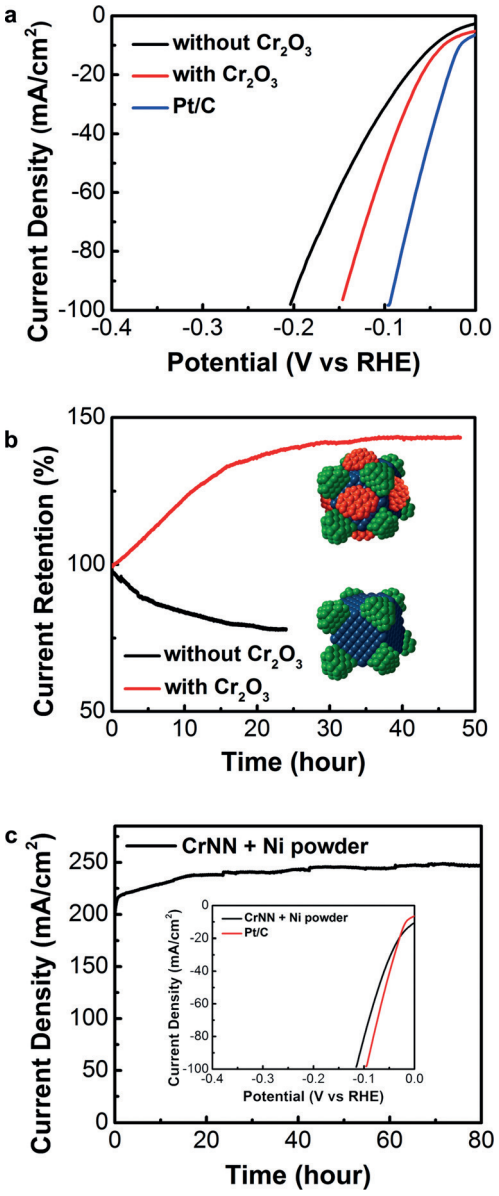

Figure 2. a) Linear sweep voltammetry (LSV) curves of the NiO/Ni heterostructure with and without Cr_2O_3 blending and Pt/C in 1 M KOH (loading of 8 mg cm^2) without *iR* compensation ($R \approx 0.5$ Ohm). b) Chronoamperometry curves of NiO/Ni heterostructure with and without Cr_2O_3 blending with initial current densities of 20 mA cm^{-2}. c) Chronoamperometry curves of the CrNN catalyst (loading of 24 mg cm^{-2}) with 30 wt% Ni powder at constant potential of −0.25 V versus RHE without *iR* compensation ($R \approx 0.6$ Ohm). Inset shows LSV curves of CrNN catalyst with 30 wt% Ni powder compared to Pt/C without *iR* compensation.

ing Information) revealed 3–10 nm metallic Ni cores coated by a 1–2 nm thick layer of nickel oxide (NiO_x) partitioned by 1–2 nm chromium oxide (CrO_x) domains (Figure 1c–f). Depth profiling X-ray photoelectron spectroscopy (XPS) further confirmed the +2 and +3 oxidation states of Ni and Cr, respectively, in the oxide layer, and the inner metallic Ni core when the oxide layer was removed by in situ Ar sputtering (Figure S2). Thus, the structure of the catalyst was nanoscale Ni cores covered by a thin layer of mixed Cr_2O_3 and NiO phases (Figure 1b). Notably, the metal-foam substrate was found to substantially impact on forming the catalyst structure (see the Supporting Information).

In 1M KOH, the CrNN electrocatalyst showed zero overpotential at the HER onset and 150 mV overpotential to reach a current density of 100 mA cm^{-2} without *iR* compensation, which is similar to commercial Pt/C under similar loading (Figure 2a). Significant improvement in steeper rise in the *iV* curve at high overpotentials was observed over NiO/Ni heterostructure (Figure 2a), possibly attributed to larger electrochemical surface area of the CrNN catalyst as indicated by the larger $Ni^{2+}/Ni^{\delta+}$ ($\delta \geq 3$) redox peak area (Figure 3c and f).

Cr_2O_3 blending significantly impacts the HER stability of the CrNN catalyst. Under constant voltage operation, the

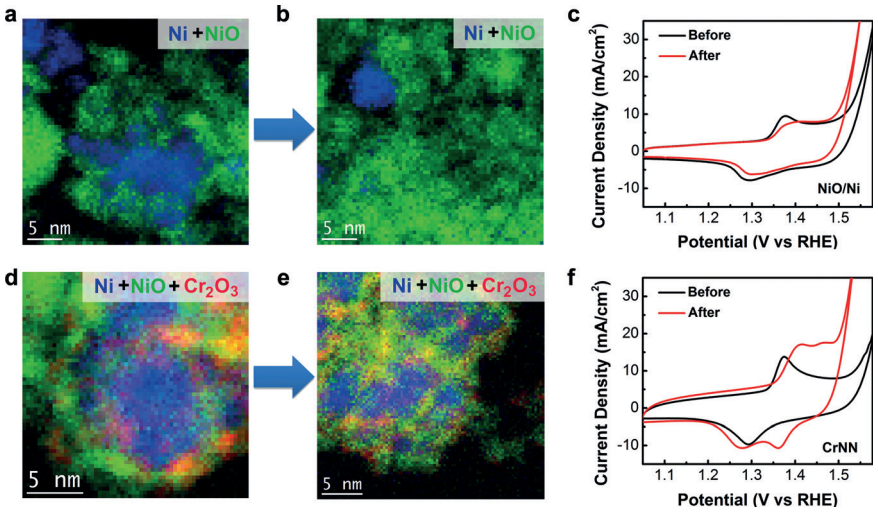

Figure 3. a,b) High-magnification STEM-EELS chemical maps for the spatial distribution of Ni, NiO and their overlays in the NiO/Ni heterostructure a) before and b) after the stability test showing severe oxidation of metallic Ni component. c) Cyclic voltammetry curves (second cycle) of NiO/Ni heterostructure before and after stability test at a scan rate of 10 mV s^{-1} in 1 M KOH. The active metallic Ni species were converted into Ni^{2+} species once biased at positive potentials (see first cycle in Figure S6). d,e) High-magnification STEM-EELS chemical maps for the spatial distribution of Ni, NiO, Cr_2O_3 and their overlays in the CrNN catalyst d) before and e) after the stability test showing intact structure. f) Cyclic voltammetry curves (second cycle) of the CrNN catalyst before and after stability test at a scan rate of 10 mV s^{-1} in 1 M KOH, showing the formation of an oxidation-resistant Ni species. The catalysts for STEM-EELS mapping were sonicated off from the Ni foam before and after stability measurement. The catalyst electrode after sonication showed dramatically decreased activity (Figure S7), suggesting that the HER activity was mainly from the catalyst and the STEM-EELS mapping result fully represented the morphology and composition of the catalyst before and after the stability measurement.

NiO/Ni electrocatalyst showed a gradual decrease in current density suggesting catalyst degradation, while 10% Cr_2O_3 greatly stabilized the catalyst with an initially increasing current density through an activation phase over 48 h and a stable current density afterwards (Figure 2b). We also investigated the catalytic activity and stability of CrNN catalysts with different Cr_2O_3 content. A low Cr_2O_3 content of 5% led to a slight decay in the current density over HER operation but increasing the Cr_2O_3 content to 20% decreased the HER activity possibly by excessive Cr_2O_3 coating blocking the HER active Ni sites (Figure S3).

To glean the mechanism of stabilizing effect and initial activation stage related to Cr_2O_3, we investigated the composition, morphology, and structure of the catalyst before and after long electrolysis tests by STEM imaging and EELS mapping (Figure 3). The NiO/Ni heterostructures without any Cr added showed significant particle oxidation into larger NiO aggregates over 24 h HER operation (Figure 3a and b), likely by oxygen dissolved in the electrolyte or oxygen migrated from the counter electrodes. The activity loss was attributed to the loss of metallic Ni content and active NiO/Ni interfaces, as H adsorption sites at the NiO/Ni interface on the metallic Ni side was proposed to be responsible for a high HER activity of the NiO/Ni catalyst.[3d] In contrast, the CrNN catalyst showed negligible particle oxidation with an almost intact NiO/Ni core structure after 48 h electrolysis operation at −60 mV versus reversible hydrogen electrode (RHE; 20–30 mA cm^{-2}) through a long stability test (Figure 3d and e). The intact NiO/Ni chemical property was further confirmed by XPS analysis (Figure S4). As Cr_2O_3 was chemically stable under the pH and potential range of the HER operation according to the Pourbaix diagram,[8] the Cr_2O_3 phase served as excellent protection for the NiO/Ni heterostructures, preventing oxygen penetration to oxidize the Ni core and maintaining the NiO/Ni heterostructure for active HER catalysis.

An interesting change in the detailed chemical structure of the catalyst was that after long HER operation, the Cr_2O_3 phase showed a tendency to co-localize with the NiO phase according to atomic-scale high-resolution EELS mapping (Figure S5). This suggested that part of the Cr_2O_3 phase was possibly blended into the NiO phase to form $NiCrO_x$ surrounding the metallic Ni nanocores. By comparing the peak areas of $Ni^{2+}/Ni^{\delta+}$ ($\delta \geq 3$) redox peak before and after 48 h of HER reaction, we observed a slightly increased electrochemical surface area by 1.23 times for the CrNN electrocatalyst (Figure 3f), which corroborated with the activation stage during which rearrangement of the oxide layer occurred to form $NiCrO_x$ during HER, allowing for higher accessibility of the Ni catalytic sites to the electrolyte. In contrast, the NiO/Ni catalyst without Cr_2O_3 after long HER operations showed a decreased electrochemical surface area, which corroborated with the loss of active NiO/Ni sites (Figure 3b) and consequently the slow decay in HER activity (Figure 2b).

Also interesting was that after long HER electrocatalysis with the CrNN catalyst, the $Ni^{2+}/Ni^{\delta+}$ ($\delta \geq 3$) redox peak of the catalyst split into two separate peaks with one of the peaks shifting to a more positive potential, indicating two distinct Ni^{2+} species in the CrNN catalyst including a more reactive one and a more inert or oxidation-resistant one (Figure 3f). We attributed the two peaks to Ni^{2+} oxidation from NiO or $Ni(OH)_2$ (resulting from oxidation of the metallic Ni phase in the catalyst) without Cr_2O_3 blending and Ni^{2+} oxidation in the $NiCrO_x$ layer, respectively.

We intentionally added Ni powder during drop drying of reaction precursors into a Ni foam and obtained improved electrocatalytic performance. An optimal loading of 24 mg cm^{-2} CrNN catalyst with 30 wt% Ni powder in Ni foam could yield a current density of 100 mA cm^{-2} at an overpotential of 115 mV without *iR* compensation (Figure 2c inset and Figure S8). Attractively, the catalyst also exhibited stable behavior in maintaining current density over 200 mA cm^{-2} for at least 80 h at −250 mV versus RHE without *iR* compensation (Figure 2c). With its superior

activity and excellent stability, the CrNN catalyst holds high promise as the cathode material for water splitting and the chloralkali industry.

We paired up the CrNN HER electrocatalyst with a high performance NiFe layered double hydroxide (LDH) oxygen-evolution reaction electro-catalyst[5c] in 1M KOH to make an alkaline electrolyzer. To match the loading of material on the HER side, we increased the loading of NiFe LDH to 20 mg cm^{-2} with addition of 30 wt% Ni powder to improve the charge transport. At room temperature (RT, 23°C), the electrolyzer impressively delivered a water splitting current at an onset voltage of 1.46 V, and a high current density of 200 mA cm^{-2} at 1.75 V without *iR* compensation (1.57 V with *iR* compensation; Figure 4b). At 60°C, the curves shifted by 100 mV to lower voltages with a 1.39 V onset potential and 1.64 V at the current density of 200 mA cm^{-2}. Our electrodes outperformed the standard Ni and stainless-steel pair used in industrial alkaline electrolyzers[3a,f] by 510 mV under RT and 370 mV at 60°C, corresponding to 22.6% and 18.4% savings of voltage and energy, respectively (Figure 4b).

The electrolyzer was stable at a current density of 20 mA cm^{-2} under a nearly constant voltage of 1.50 V (without *iR* compensation) over 500 h (Figure 4c). It also showed negligible decay under a high current density of 200 mA cm^{-2} for 50 h under 1.75 V and 1.64 V at RT and 60°C, respectively (Figure 4c).

The conversion of solar energy directly into hydrogen fuels by water photolysis is a promising route of energy conversion and storage.[9] Aimed at water photolyzers with high efficiency, we employed state of the art thin-film GaAs solar cells.[10] GaAs has a suitable direct band gap leading to a large open circuit voltage and a high filled factor (Table S1), which makes it impelling for powering the water electrolyzer. By connecting our electrolyzer with two GaAs solar cells in series (Figure 4a), we were able to produce a high current density of 12.10 mA cm^{-2} (Figure 4d) corresponding to a solar-to-hydrogen efficiency of 14.9% under AM1.5 100 mW cm^{-2} assuming a faradaic efficiency of 100% (from long-term stability). Interestingly, under lower power density of 20 mW cm^{-2} by LED desk light, the device could still deliver a current density of 2.45 mA cm^{-2} (Figure 4d) corresponding to a solar-to-hydrogen efficiency of 15.1%, which implies that we can make use of the wasted light energy for H_2 conversion at night. Due to the stable behavior of GaAs solar cell and our electrolyzer, the device was able to maintain almost the same current density over more than 24 h under both sun simulator and LED desk light (Figure 4e).

In conclusion, we discovered Cr_2O_3-blended NiO/Ni heterostructures as highly active HER catalysts with sustained H_2 production over long operations. The Cr_2O_3 on the surface was found to be essential for maintaining the core NiO/Ni active sites from oxidation and aggregation. Cr_2O_3 blended into NiO to form chemically inert $NiCrO_x$ during HER, which improves the HER activity and stability by inducing larger electrochemical surface area and increasing oxygen resistance. The CrNN catalyst could afford a current density of 100 mA cm^{-2} at 115 mV overpotential with long-term stability. Pairing of the HER catalyst with NiFe LDH

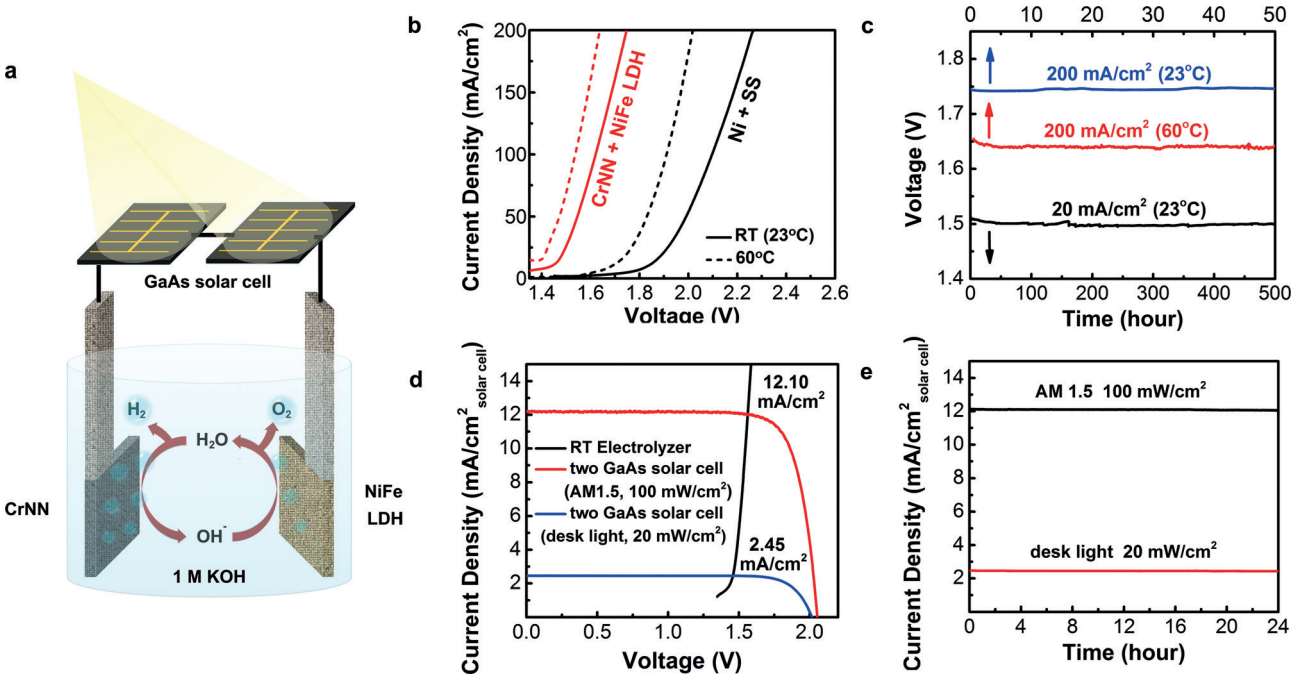

Figure 4. a) Schematic diagram of solar-driven water splitting using two GaAs solar cell in series and alkaline electrolyzer with CrNN and NiFe LDH catalysts. b) LSV curves of the electrolyzer using CrNN catalyst as cathode (24 mg cm^{-2}, 30 wt% Ni powder) and NiFe LDH as anode (20 mg cm^{-2}, 30 wt% Ni powder) compared to Ni cathode and stainless steel (SS) anode under room temperature (RT, 23°C) and 60°C without *iR* compensation ($R \approx 0.9$ Ohm). c) Chronopotentiometry curves of the electrolyzer with CrNN and NiFe LDH catalysts at constant current densities under RT and 60°C without *iR* compensation. d) Solar cell *i*–*V* curves of GaAs solar cell under simulated AM 1.5 100 mW cm^{-2} and LED desk light 20 mW cm^{-2} illumination overlapping with electrolyzer *i*–*V* curves. e) Current density versus time curve of the GaAs solar-cell-driven water splitting.

anode enables water electrolyzer and photolyzer with superior efficiency and stability.

Acknowledgements

This work was supported by a grant from Stanford GCEP, a Steinhart/Reed Award from the Stanford Precourt Institute for Energy, the Global Networking Talent 3.0 plan (NTUST 104DI005) from the Ministry of Education of Taiwan and by the U.S. Department of Energy, Office of Basic Energy Sciences, Division of Materials Sciences and Engineering under award number DOE DE-SC0008684 (for carbon nanomaterials synthesis and characterization with advanced electrical properties). The electron microscopy study was supported by the U.S. Department of Energy, Office of Science, Basic Energy Science, Materials Sciences and Engineering Division (W.Z.), and through a user project at ORNL's Center for Nanophase Materials Sciences (CNMS), which is a DOE Office of Science User Facility.

Keywords: chromium oxide · electrocatalysts · hydrogen-evolution reaction · sustainable chemistry · water splitting

How to cite: *Angew. Chem. Int. Ed.* **2015**, *54*, 11989–11993
Angew. Chem. **2015**, *127*, 12157–12161

[1] a) G. W. Crabtree, M. S. Dresselhaus, M. V. Buchanan, *Phys. Today* **2004**, *57*, 39–44; b) M. S. Dresselhaus, I. L. Thomas, *Nature* **2001**, *414*, 332–337; c) D. G. Nocera, *Acc. Chem. Res.* **2012**, *45*, 767–776; d) M. G. Walter, E. L. Warren, J. R. McKone, S. W. Boettcher, Q. Mi, E. A. Santori, N. S. Lewis, *Chem. Rev.* **2010**, *110*, 6446–6473.

[2] P. Häussinger, R. Lohmüller, A. M. Watson, *Ullmann's Encyclopedia of Industrial Chemistry*, Wiley-VCH, Weinheim, **2000**.

[3] a) M. Carmo, D. L. Fritz, J. Merge, D. Stolten, *Int. J. Hydrogen Energy* **2013**, *38*, 4901–4934; b) C. L. Choi, J. Feng, Y. Li, J. Wu, A. Zak, R. Tenne, H. Dai, *Nano Res.* **2013**, *6*, 921–928; Y. Zhang, J. Shi, G. Han, M. Li, Q. Ji, D. Ma, Y. Zhang, C. Li, X. Lang, Y. Zhang, *Nano Res.* **2015**, *8*, 1–10; c) J. Feng, M. Gong, M. Kenney, J. Wu, B. Zhang, Y. Li, H. Dai, *Nano Res.* **2015**, *8*, 1–7; d) M. Gong, W. Zhou, M.-C. Tsai, J. Zhou, M. Guan, M.-C. Lin, B. Zhang, Y. Hu, D.-Y. Wang, J. Yang, S. J. Pennycook, B.-J. Hwang, H. Dai, *Nat. Commun.* **2014**, *5*, 0; e) M. J. Kenney, M. Gong, Y. Li, J. Z. Wu, J. Feng, M. Lanza, H. Dai, *Science* **2013**, *342*, 836–840; f) K. Zeng, D. Zhang, *Prog. Energy Combust. Sci.* **2010**, *36*, 307–326.

[4] Y. Liang, Y. Li, H. Wang, H. Dai, *J. Am. Chem. Soc.* **2013**, *135*, 2013–2036.

[5] a) D. Friebel, M. W. Louie, M. Bajdich, K. E. Sanwald, Y. Cai, A. M. Wise, M.-J. Cheng, D. Sokaras, T.-C. Weng, R. Alonso-Mori, R. C. Davis, J. R. Bargar, J. K. Nørskov, A. Nilsson, A. T. Bell, *J. Am. Chem. Soc.* **2015**, *137*, 1305–1313; b) M. Gong, H. Dai, *Nano Res.* **2015**, *8*, 23–39; c) M. Gong, Y. Li, H. Wang, Y. Liang, J. Z. Wu, J. Zhou, J. Wang, T. Regier, F. Wei, H. Dai, *J. Am. Chem. Soc.* **2013**, *135*, 8452–8455; d) M. W. Kanan, D. G. Nocera, *Science* **2008**, *321*, 1072–1075; e) E. J. Popczun, J. R. McKone, C. G. Read, A. J. Biacchi, A. M. Wiltrout, N. S. Lewis, R. E. Schaak, *J. Am. Chem. Soc.* **2013**, *135*, 9267–9270; f) J. Suntivich, K. J. May, H. A. Gasteiger, J. B. Goodenough, Y. Shao-Horn, *Science* **2011**, *334*, 1383–1385; g) D.-Y. Wang, M. Gong, H.-L. Chou, C.-J. Pan, H.-A. Chen, Y. Wu, M.-C. Lin, M. Guan, J. Yang, C.-W. Chen, Y.-L. Wang, B.-J. Hwang, C.-C. Chen, H. Dai, *J. Am. Chem. Soc.* **2015**, *137*, 1587–1592.

[6] a) Y. Sun, M. Delucchi, J. Ogden, *Int. J. Hydrogen Energy* **2011**, *36*, 11116–11127; b) J. R. McKone, S. C. Marinescu, B. S. Brunschwig, J. R. Winkler, H. B. Gray, *Chem. Sci.* **2014**, *5*, 865–878.

[7] a) I. Olefjord, *Mater. Sci. Eng.* **1980**, *42*, 161–171; b) M. F. Montemor, M. G. S. Ferreira, N. E. Hakiki, M. D. Belo, *Corros. Sci.* **2000**, *42*, 1635–1650; c) P. Stefanov, D. Stoychev, M. Stoycheva, T. Marinova, *Mater. Chem. Phys.* **2000**, *65*, 212–215.

[8] B. Beverskog, I. Puigdomenech, *Corros. Sci.* **1997**, *39*, 43–57.

[9] a) C. R. Cox, J. Z. Lee, D. G. Nocera, T. Buonassisi, *Proc. Natl. Acad. Sci. USA* **2014**, *111*, 14057–14061; b) J. Luo, J.-H. Im, M. T. Mayer, M. Schreier, M. K. Nazeeruddin, N.-G. Park, S. D. Tilley, H. J. Fan, M. Graetzel, *Science* **2014**, *345*, 1593–1596.

[10] a) M. A. Green, K. Emery, Y. Hishikawa, W. Warta, E. D. Dunlop, *Prog. Photovoltaics* **2015**, *23*, 1–9; b) O. Khaselev, J. A. Turner, *Science* **1998**, *280*, 425–427.

Received: May 31, 2015
Revised: July 9, 2015
Published online: August 24, 2015

